Superhydrophobic metallic surfaces functionalized via femtosecond laser surface processing for long term air film retention when submerged in liquid

Craig A. Zuhlke*[a], Troy P. Anderson[a], Pengbo Li[b], Michael J. Lucis[b], Nick Roth[a], Jeffery E. Shield[b], Benjamin Terry[b], Dennis R. Alexander[a]

[a]Department of Computer and Electrical Engineering, [b]Department of Mechanical and Materials Engineering, University of Nebraska-Lincoln, 844 N 16th St, Lincoln, NE USA 68588

ABSTRACT

Femtosecond laser surface processing (FLSP) is a powerful technique used to create self-organized microstructures with nanoscale features on metallic surfaces. By combining FLSP surface texturing with surface chemistry changes, either induced by the femtosecond laser during processing or introduced through post processing techniques, the wetting properties of metals can be altered. In this work, FLSP is demonstrated as a technique to create superhydrophobic surfaces on grade 2 titanium and 304 stainless steel that can retain an air film (plastron) between the surface and a surrounding liquid when completely submerged. It is shown that the plastron lifetime when submerged in distilled water or synthetic stomach acid is critically dependent on the specific degree of surface micro- and nano-roughness, which can be tuned by controlling various FLSP parameters. The longest plastron lifetime was on a 304 stainless steel sample that was submerged in distilled water and maintained a plastron for 41 days, the length of time of the study, with no signs of degradation. Also demonstrated for the first time is the precise control of pulse fluence and pulse count to produce three unique classes of surface micron/nano-structuring on titanium.

Keywords: femtosecond laser; ultrashort laser; laser microstructuring; wetting properties; plastron; superhydrophobic

1. INTRODUCTION

Superhydrophobic surfaces that can retain an air film (plastron) when submerged in liquid have many promising applications ranging from drag reduction[1] to antifouling by creating a boundary between fouling agents and the sample surface[2]. One of the greatest challenges to the application of superhydrophobic surfaces for antifouling applications is the limited lifetime of the generated plastron. Plastrons on insects submerged in water have been observed by other research groups to be stable for several months[3,4], but engineered surfaces have resulted in much shorter lifetimes[5]. In this work we demonstrate that the lifetime of a plastron is dependent on the degree of surface micro/nanostructuring as well as the composition of the base material. The longest plastron lifetime presented in this work is on a 304 SS surface that had an undisturbed plastron present after being submerged in distilled water to a depth of 30 mm for 41 days.

A superhydrophobic surface requires two critical aspects: the creation of large surface area, and a hydrophobic interfacial surface. Femtosecond lasers are developing into a common tool for producing high surface area, micro/nanostructured surfaces on a wide range of materials. Examples of self-organized surface structures that have been demonstrated using femtosecond laser surface processing (FLSP) include pillars[6–9], cones[10–12], spikes[8,13–15], mounds[16,17], and pyramids[17,18]. We have previously utilized this technique to study the formation of three unique surface structures on nickel and 304 stainless steel (SS): above surface growth mounds (ASG-mounds), below surface growth mounds (BSG-mounds) and nanoparticle covered pyramids (NC-pyramids)[16–21]. In this work, we present for the first time utilizing precise control of the pulse fluence and pulse count to create these three unique classes of structures on titanium.

2. EXPERIMENT

2.1 Sample Fabrication

A Femtosecond Laser Surface Processing (FLSP) technique was used to create quasiperiodic microstructures covered in layers of nanoparticles on 304 stainless steel (SS) and grade 2 titanium (Ti). Surface features generated using the FLSP technique are formed through self-organization processes induced by the femtosecond laser ablation pulses. The size and

Laser-based Micro- and Nanoprocessing IX, edited by Udo Klotzbach, Proc. of SPIE Vol. 9351, 93510J · © 2015 SPIE · CCC code: 0277-786X/15/$18 · doi: 10.1117/12.2079164

shape of the features are controlled through the laser fluence, and the number of laser pulses per area incident on the sample.

The FLSP setup can be seen in Figure 1a. The laser used for this work was a Spitfire, Ti:Sapphire laser system from Spectra Physics capable of producing 1 mJ, 80 fs pulses at a 1 kHz repetition rate. The laser pulses were monitored using a Frequency Resolved Optical Gating (FROG) instrument from Positive Light (Model 8-02). The pulses were focused using a 152.4 mm focal length parabolic mirror (MPD254762-90-P01). The samples were placed on computer-controlled 3D translation stages and raster scanned through the beam path of the laser in order to process an area larger than the laser spot size. The number of pulses incident on the sample was controlled by adjusting the translation speed of the sample and the pitch between raster scans. The samples used in the work were cut to 1 cm x 2 cm rectangles and half of each sample was processed. An example of a processed Ti sample can be seen in Figure 1b. As a side effect of FLSP, all 304 SS samples turned black, while the processed Ti samples turned a bluish color. Before processing all samples were given an acetone rinse followed by a 5 minute ultrasonic bath in distilled water.

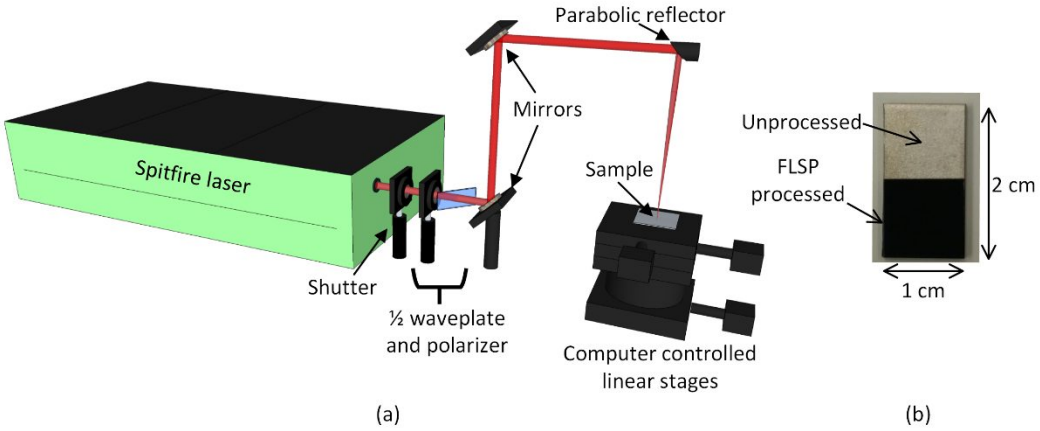

Figure 1: (left) FLSP setup. (right) Optical image of an example FLSP processed titanium sample.

The resulting surfaces after the FLSP procedure were superhydrophilic due to the hydrophilic nature of the 304 SS and Ti surfaces. In order alter the surface chemistry to produce superhydrophobic surfaces, the samples were stored in a vacuum chamber at 3 x 10^{-6} mbar for 18 days. Although the process resulting in the change in wetting properties from the vacuum chamber is not completely understood, we hypothesize that hydrocarbons from the rotary vane vacuum pumps (Edwards RV8) are vaporized at low vacuum pressures, below the vapor pressure for the hydrocarbons in the vacuum pump oils, and enters the chamber via back-streaming. In the vacuum chamber the hydrocarbons are then adsorbed to the sample surface. The inherently hydrophobic hydrocarbons coat the micro/nanoscale hierarchical structures resulting in a superhydrophobic surface. The vacuum pumps use Edwards Grade 19 pump oil.

2.2 Surface analysis

The surfaces were characterized with the use of scanning electron microscopes (SEM) and a laser scanning confocal microscope (Keyence VK-X100). SEM images were taken using both a Philips XL-30 Environmental Scanning Electron Microscope (SEM), and a Helios 660 both manufactured by FEI Company. EDX measurements were carried out using a EDAX SDD Octane Super EDS detector in the Helios 660 SEM. Contact angles were taken using a Rame-Hart Model 590 F4 Series Goniometer and Tensiometer.

2.3 Fabricated samples

Through FLSP, three unique classes of textured surfaces were produced on both 304 SS and Ti. The three structure classes produced, ASG-mounds, BSG-mounds and NC-pyramids, have previously been demonstrated on 304 SS[19–21] and nickel[16–18,22]. Although mound-like structures have been demonstrated in the past on Ti[23–26], this is the first time to our knowledge that precise control over the applied laser parameters was used to generate the three unique structure classes presented in this work. Each of these types of surfaces have been described in detail in previous publications and form through a combination of preferential ablation processes, capillary flow of laser-induced melt layers, and redeposition of ablation material in the form of solid material and nanoparticles created during the ablation process. The balance of these formation

processes leading to unique structures is determined by the fluence of the ablation pulses, and the pulse count on the sample.

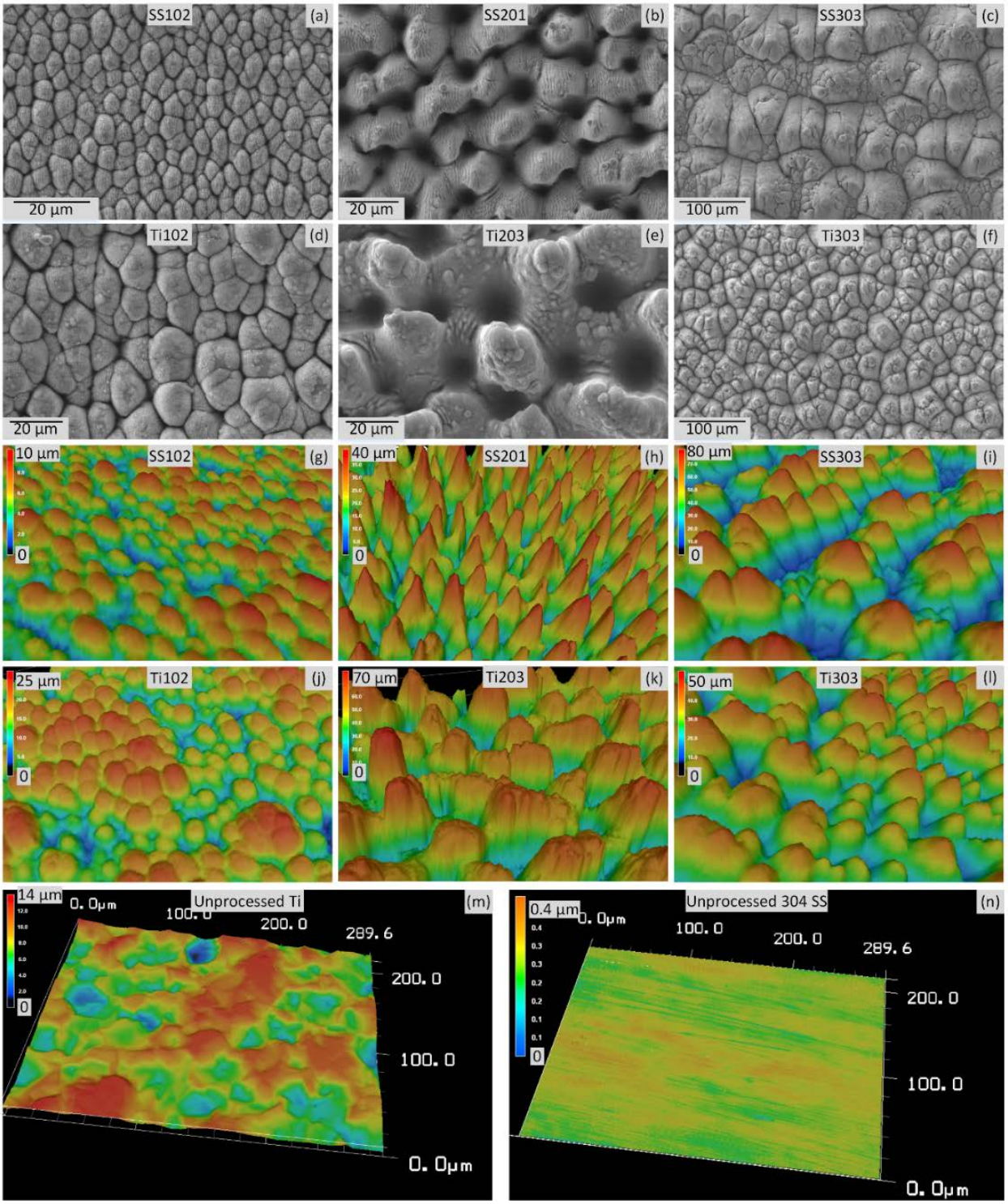

Figure 2: (a-f) SEM images and (g-l) 3D profiles of FLSP processed surfaces. The 304 SS surface structures types are (a, g) BSG-mounds (b, h) ASG-mounds, and (c, i) NC-pyramids. The Ti surface structures are (d, j) BSG-mounds (e, k) ASG-mounds, and (f, l) NC-pyramids. (m, n) 3D profiles of unprocessed (m) Ti and (n) 304 SS.

Each structure class has unique physical characteristics and it has been shown that the contact angle for FLSP processed surfaces is dependent on the specific morphology produced[27]. Therefore, each structure class was produced on both 304 SS and Ti to determine if the various structure and material combinations would result in different plastron lifetimes when submerged in both distilled water and synthetic stomach acid. SEM images and 3D profiles of each type of structure produced can be seen in Figure 2, along with the 3D profiles of unprocessed surfaces. It should be noted that the 3D profiles in Figure 2 are at different magnifications and can be used to compare structure characteristics (aspect ratio, density etc.), but not structure sizes. Not visible at the magnifications shown here are layers of nanoparticles that overlay each surface as discussed in previous publications[17,19]. NC-pyramids have the thickest layer of nanoparticles on the surface and has been shown to be as thick as several microns[19]. BSG-mounds and ASG-mounds are covered in a thinner layer of nanoparticles[17], with BSG-mounds generally having a more uniform coverage than ASG-mounds.

For each of the surfaces produced, the surface roughness, peak-to-valley height, and surface area ratio were measured using the Keyence laser confocal microscope. Structure peak spacing was determined by taking a 2D Fast Fourier Transform (FFT) of SEM images in Matlab. The parameters used to produce each surface along with the measured geometric parameters are included in Table 1. The laser spot size on the sample, used to calculate values in Table 1, was determined by using the confocal microscope to measure the diameter of the ablation craters produced with 100 incident pulses at a range of input powers, a method outlined by Bonse et. al.[28] Although the physical parameters of the structures produced on 304 SS and Ti for each structure type are not identical, it is expected that if a full parameter study was carried out on each material that closer matching structures could be produced.

Table 1: Sample design parameters and physical parameters.

Sample name	Design parameters			Measured physical parameters				
	Structure type	Peak fluence (J/cm^2)	Pulse count	Average roughness (µm)	Average structure height (µm)	Maximum structure height (max peak to max valley) (µm)	Surface area ratio (measured surface area/geometric area) (µm)	Structure peak spacing (µm)
Unprocessed SS	-	-	-	0.0	-	-	1.0	-
SS102 SS104	BSG-mounds	1.8	328	1.6	6.9	11.0	2.4	8.0
SS201 SS202	ASG-mounds	4.4	242	7.4	30.6	42.1	4.8	24.2
SS303 SS304	NC-pyramids	0.3	14448	16.0	69.2	81.9	2.9	84.1
Unprocessed Ti	-	-	-	2.2	5.4	14.1	1.2	-
Ti102 Ti103	BSG-mounds	1.6	369	3.7	12.0	28.8	2.5	15.3
Ti202 Ti203	ASG-mounds	4.2	252	14.1	62.0	80.3	4.7	30.2
Ti302 Ti303	NC-pyramids	0.3	14810	7.6	38.1	54.7	3.2	41.7

2.4 Plastron lifetime analysis

A time lapse imaging technique was used to quantify the lifetime of the plastron for each surface. One set of FLSP functionalized surfaces was submerged in distilled water and another set was submerged in synthetic stomach acid: Artificial Gastric Juice, item number 470301-128 from Ward's Science. The experimental setup for imaging the plastron is diagrammed in Figure 3. The liquid was contained in a clear acrylic box and a lamp, with lens tissue used to diffuse the light, was used to illuminate the samples on the opposite side of viewing. With this setup the plastron is visible due to a mirror-like reflection at the water-air interface. As the plastron degrades this reflection decreases, and once the plastron is

completely degraded the original color of the FLSP functionalized surface is visible. After full plastron degradation the 304 SS samples appeared black and the Ti samples appeared a bluish color. A computer controlled Fuji Film S5 Pro DSLR camera was used to capture images of the plastron at regular time intervals. The water and synthetic stomach acid levels were maintained at 30 mm above the top of the sample with liquid added over time to counteract evaporation.

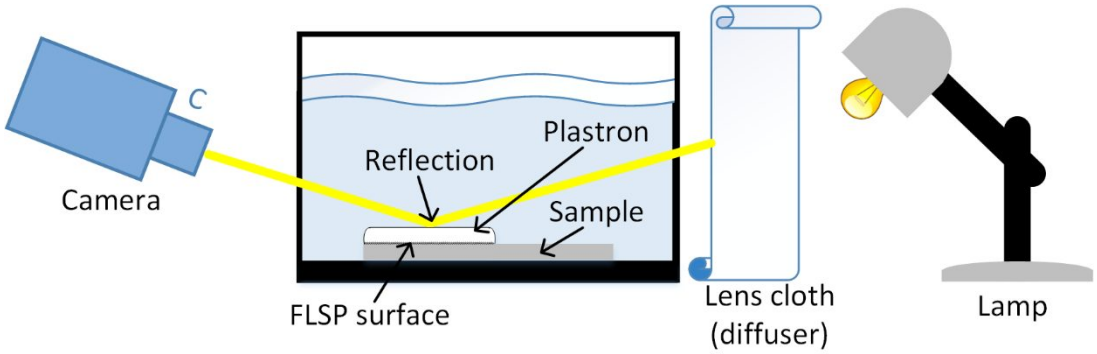

Figure 3: Experimental setup for imaging plastron on FLSP functionalized surface.

Once the samples were submerged, the plastron degraded slowly over time and at different rates for each sample. As a method to compare the plastron degradation between samples, the time for two stages of degradation was recorded. Examples of the stages of degradation can be seen in Figure 4. When first submerged, all the surfaces produced a uniform plastron evident by a uniform, highly reflective surface as seen in Figure 4a. The first time stamp noted was for a partially degraded plastron as seen in Figure 4b, which is discernable by a visible decrease in reflection and a non-uniform plastron surface. The second time stamp noted was for complete degradation of the plastron. At complete degradation the surface appeared the color of the FLSP modified surface as seen in Figure 4c. It should be noted that at the time considered as complete degradation, an air bubble often remained attached to the surface. These air bubbles would also eventually degrade leaving a completely wetted surface.

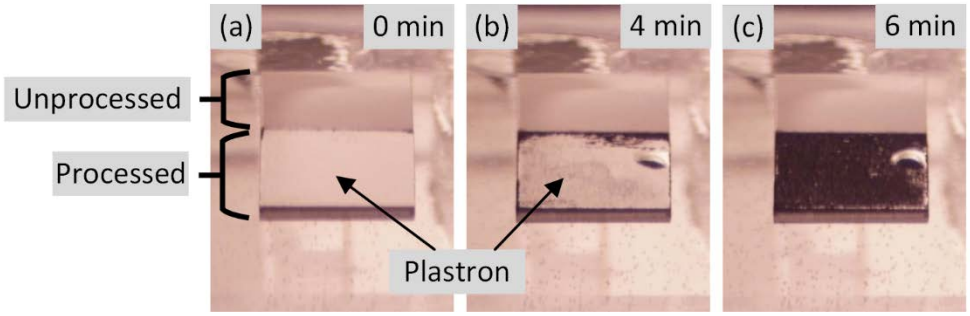

Figure 4: Optical images of plastron degradation over time on sample SS202 submerged in synthetic stomach acid, where (a) is a fully developed plastron after initial immersion, (b) is a partially degraded plastron and (c) is a fully degraded plastron.

The contact angle of the surfaces was taken after being placed in the vacuum chamber, and a second time after the samples were submerged and the plastron had fully degraded. Contact angles were not taken for these surfaces before time in the vacuum chamber, because immediately after FLSP processing these types of surfaces are superhydrophilic/superwicking[19,20] and checking contact angles could affect the surface chemistry. Each contact angle and roll off angle included in this paper are the average of measurements taken at three locations on the sample. All contact angles were taken using 6 µL droplets of distilled water.

3. RESULTS AND DISCUSSION

Table 2 contains the results for the plastron lifetimes in both distilled water and synthetic stomach acid, as well as the contact angles before and after submerging the samples. After 18 days in the vacuum chamber, all but one sample was

determined to be superhydrophobic based on the commonly referenced values of contact angles greater than 150 degrees and roll off angles less than 10 degrees[29]. It is unclear why Ti103 had a larger roll off angle and smaller contact angle than the other samples, but it may have been due to non-uniform coating of samples depending on location within the vacuum chamber.

Table 2: Contact angles and plastron lifetimes. The contact and roll off angles are stated as the mean ± standard error.

SAMPLE	Wetting properties				Plastron Lifetime (days:hours:minutes)	
	After 18 days in vacuum chamber		After plastron degradation	Total time submerged	Partially degraded	Fully degraded
	Contact angle (degrees)	Roll off angle (degrees)	Contact angle (degrees)			
Submerged in water						
SS102	168 ± 3	1 ± 1	27 ± 6	41 days	27:06:33	39:22:41
SS201	165 ± 3	3 ± 2	-	41 days	>41 days	>41 days
SS303	163 ± 3	5 ± 2	121 ± 11	3 days	00:01:20	00:04:51
Ti102	162 ± 3	4 ± 2	17 ± 5	29 days	00:02:01	03:23:22
Ti203	162 ± 3	4 ± 1	111 ± 5	3 days	00:00:28	00:01:16
Ti303	162 ± 3	3 ± 2	67 ± 6	12 days	00:08:53	11:08:58
Submerged in synthetic stomach acid						
SS104	161 ± 4	4 ± 1	99 ± 4	2 days	00:00:05	00:00:10
SS202	164 ± 2	2 ± 1	122 ± 9	7 min	00:00:04	00:00:06
SS304	162 ± 2	1 ± 1	51 ± 11	2 days	00:00:01	00:00:03
Ti103	158 ± 2	23 ± 22	115 ± 3	190 min	00:00:10	00:00:54
Ti202	159 ± 2	8 ± 1	114 ± 9	3 days	00:00:09	00:00:35
Ti302	162 ± 3	9 ± 1	81 ± 2	3 days	00:00:19	00:01:19

The plastron lifetimes in both distilled water and synthetic stomach acid ranged from minutes to longer than a month, depending on the sample. Sample SS201 (ASG-mounds on 304 SS), submerged in distilled water, resulted in the longest plastron lifetime with a full plastron still present after 41 days, the length of time for this study, with no signs of degradation. For both water and stomach acid the plastron lifetime followed similar trends in the terms of the performance based on structure class. On 304 SS, the plastron on the ASG- and BSG-mounds lasted the longest and the plastron on the NC-pyramids had the shortest lifetime when submerged in both distilled water and synthetic stomach acid. For Ti, the NC-pyramids had the longest lifetime followed by BSG-mounds and then ASG-mounds in both distilled water and synthetic stomach acid. There is not a clear trend based on the measured parameters to predict this order of plastron lifetimes. A parameter that could affect this lifetime that is not easily quantifiable is the regularity of structure peaks in relation to both height and spacing. By comparing SEM images as well as 3D profiles the regularity of the peaks in terms of height and spacing appears to be for 304 SS: (1) ASG-mounds, (2) BSG-mounds, (3) NC-pyramids and for Ti: (1) NC-pyramids, (2) BSG-mounds, (3) ASG-mounds. If the plastron is resting on the peaks of the structures[30] than a greater regularity of the peaks would result in a more uniform plastron. An irregular plastron, resulting from irregular peaks, could lead to localized degradation and an overall higher rate of degradation.

Although there is no clear correlation between the plastron lifetime and any of the measured parameters included in this paper, it is evident that the plastron lifetime is dependent on the morphology of the textured surfaces. There are a number of factors, not quantified in this study, that vary between individual samples and can affect this lifetime. A few include:

1. the thickness of the nanoparticle layer overlaying the microstructures: this thickness would affect both the rate of hydrocarbon adsorption as well as the amount of surface area interacting with the water
2. the regularity of the peaks in both height and spacing
3. the sharpness or bluntness of the structure peaks

On average among this series of samples, the 304 SS maintained a plastron for the longest period of time in distilled water, while the Ti surfaces maintained a plastron longest in the synthetic stomach acid. Since both materials are coated with the same hydrocarbon layer, it was expected that the relative lifetimes between samples would be similar when

submerged in the two liquids. However, these results indicate that the liquid is interacting with the base material. It is unclear if the interaction is immediate or if it only takes place after initial breakdown of the hydrocarbon layer upon partial depletion of the plastron. The difference in lifetime when submerged in distilled water versus synthetic stomach acid may be related to corrosion resistance of each material to each liquid. 304 SS is designed to have a passivation layer resulting in greater corrosion resistant to water than Ti. However, hydrochloric acid (HCL), the active ingredient in synthetic stomach acid, breaks down both 304 SS and Ti. If upon initial degradation of the plastron, the liquid first comes in contact with the peaks of the structures[30] the reaction that occurs between the liquid and the metal could accelerate the plastron degradation by progressively breaking down the surrounding hydrocarbon layer. Since grade 2 Ti is more resistant to corrosion by HCL than 304 SS, it is expected that the Ti samples would result in a longer plastron lifetime than the 304 SS samples when submerged in synthetic stomach acid.

For a number of experimental reasons, samples were submerged for different periods of time after the plastron was depleted. Table 2 includes values for the total time submerged for each sample. Based on the data in Table 2, the contact angle of the samples after being removed from the distilled water was dependent on the time submerged. There were also four similar samples, not included in the data for this paper, that had a contact angle of zero degrees after being submerged in distilled water for 29 days. This indicates that the distilled water is slowly degrading the hydrocarbon layer after depletion of the plastron. For the samples submerged in stomach acid the contact angle did not appear to have a similar correlation between contact angle and time submerged. However, no samples were submerged in the stomach acid for up to 29 days to make a direct comparison. A more complete study on contact angle as a function of time submerged is needed to provide better correlations.

Table 3 contains results for contact angles on unprocessed 304 SS and Ti after the initial sample cleaning, after 18 days in the vacuum chamber and after being submerged in distilled water. Contact angles are not included for the unprocessed surfaces after being submerged in synthetic stomach acid because the results varied. After submerging in stomach acid a film was present on the surface that would partially wash off with when rinsed with distilled water, and the contact angles varied from 60 degrees to 95 degrees across the unprocessed 304 SS and Ti samples after being submerged in stomach acid. This may also explain the inconsistent contact angles as a function of time submerged in stomach acid for the processed surfaces. As expected, the contact angle increases a small amount for the unprocessed surfaces after time in the vacuum chamber due to the addition of the hydrocarbon layer. The small contact angle increase on the unprocessed surfaces supports the critical need for the micro/nanostructured surfaces in producing the superhydrophobic property on the surfaces.

Table 3: Contact angles for an unprocessed 304 SS and Ti samples. The contact angles are stated as the mean ± standard error.

SAMPLE	Contact angle (degrees)			
	Before vacuum chamber	**After 18 days in vacuum chamber**	**After submerging in synthetic stomach acid**	**After submerging in water for 3 days**
Unprocessed SS	81 ± 2	84 ± 5	-	72 ± 8
Unprocessed Ti	78 ± 1	80 ± 4	-	84 ± 6

In order to better understand the surface chemistry changes induced by the vacuum chamber, EDX analysis was performed on a BSG-mound 304 SS and Ti sample. The analysis was completed immediately after laser processing and again after 18 days in the vacuum chamber. The results can be seen in Table 4 for both the FLSP processed and unprocessed samples. For all four samples the amount of carbon increased after 18 days in the vacuum chamber. This carbon is likely in the form of a hydrocarbon introduced to the vacuum chamber as a result of back streaming of vaporized vacuum pump oil at the low vacuum pressures. It has been shown that various carbon based coatings on micro/nanostructured surfaces can result in superhydrophobic surfaces[31–34].

Table 4 also shows that the oxygen content increases from the time the EDX measurements were taken before and after time in the vacuum chamber. This is likely due to oxidation of the surface over time. It should be noted that the samples were exposed to open atmosphere when being transported between the SEM used for EDX measurements and the vacuum chamber. The estimated time of exposure to open atmosphere is about 3 hours. Oxidation is supported by the fact that the oxygen increase was greater on the titanium than the 304 SS. The chromium in the 304 SS acts to limit corrosion by reducing oxidation rates. After FLSP processing, the resulting nanoparticles covering the surface are made of a metal oxide and would have a low rate of further oxidation[17]. Since the initial EDX measurements were taken within a few hours after

processing, the oxidation likely takes place on the surface below the nanoparticles, which would be in a chemically unstable state after the laser ablation processes[31]. When submerged in liquid, the hydrocarbons coating the nanoparticles would be the surface interacting with the liquid, providing the hydrophobic interfacial surface and resulting in a superhydrophobic surface when combined with the high surface area of the micro/nanostructures on the surface. The increase in both carbon and oxygen is much lower on the unprocessed surfaces due to the lower surface area and an undisturbed passivation layer resulting in slower oxidation rates than the processed samples.

Table 4: EDX analysis of an FLSP surface covered with BSG-mounds before and after hydrocarbon adsorption.

	Carbon (atomic %)		Oxygen (atomic %)	
SAMPLE	**Before vacuum chamber**	**After 18 days in vacuum chamber**	**Before vacuum chamber**	**After 18 days in vacuum chamber**
SS101	9.6	25.7	16.0	19.9
Ti101	3.5	13.4	33.7	44.5
Unprocessed SS	8.0	12.6	1.2	2.1
Unprocessed Ti	5.0	8.0	2.3	4.6

4. CONCLUSION

The lifetime of a plastron on a series of 304 SS and Ti surfaces when submerged in distilled water and synthetic stomach acid was studied. The surfaces were functionalized, to different degrees, through an FLSP technique which produces self-organized, micro/nanostructured surfaces. By placing the FLSP modified surfaces in a vacuum chamber for 18 days the surfaces became superhydrophobic. EDX measurements showed an increase in the carbon content after time in the vacuum chamber. It is hypothesized that the hydrocarbons from the vacuum pump oils vaporize at low pressures, enter the chamber through back streaming and adsorb onto the sample surfaces. It was found that the plastron lifetime was dependent on the specific type of surface texturing and that the 304 SS surfaces fared better in distilled water while the Ti surfaces fared better in the synthetic stomach acid.

ACKNOWLEDGMENTS

This work has been supported by a NASA EPSCoR Grant # NNX13AB17A, a NASA Space Grant # NNX10AN62H and a grant through the Nebraska Center for Energy Sciences Research (NCESR) with funds provided by Nebraska Public Power District (NPPD) to the University of Nebraska-Lincoln (UNL) # 4200000844.

REFERENCES

[1] McHale, G., Newton, M. I.., Shirtcliffe, N. J., “Immersed superhydrophobic surfaces: Gas exchange, slip and drag reduction properties,” Soft Matter **6**(4), 714 (2010).

[2] Arnott, J., Wu, A. H. F., Vucko, M. J.., Lamb, R. N., “Marine antifouling from thin air.,” Biofouling **30**(9), 1045–1054 (2014).

[3] Balmert, A., Florian Bohn, H., Ditsche-Kuru, P.., Barthlott, W., “Dry under water: comparative morphology and functional aspects of air-retaining insect surfaces.,” J. Morphol. **272**(4), 442–451 (2011).

[4] Ditsche-Kuru, P., Schneider, E. S., Melskotte, J.-E., Brede, M., Leder, A.., Barthlott, W., “Superhydrophobic surfaces of the water bug Notonecta glauca: a model for friction reduction and air retention.,” Beilstein J. Nanotechnol. **2**, 137–144 (2011).

[5] Cheek, J., Steele, A., Bayer, I. S.., Loth, E., “Underwater saturation resistance and electrolytic functionality for superhydrophobic nanocomposites,” Colloid Polym. Sci. **291**(8), 2013–2016 (2013).

[6] Iyengar, V. V., Nayak, B. K.., Gupta, M. C., “Optical properties of silicon light trapping structures for photovoltaics,” Sol. Energy Mater. Sol. Cells **94**(12), 2251–2257, Elsevier (2010).

[7] Nayak, B. K., Gupta, M. C.., Kolasinski, K. W., “Spontaneous formation of nanospiked microstructures in germanium by femtosecond laser irradiation,” Nanotechnology **18**(19), 195302 (2007).

[8] Bonse, J., Baudach, S., Krüger, J., Kautek, W.., Lenzner, M., “Femtosecond laser ablation of silicon-modification thresholds and morphology,” Appl. Phys. A Mater. Sci. Process. **74**(1), 19–25 (2002).

[9] Kolasinski, K. W., Mills, D.., Nahidi, M., "Laser assisted and wet chemical etching of silicon nanostructures," J. Vac. Sci. Technol. A Vacuum, Surfaces, Film. **24**(4), 1474 (2006).
[10] Zorba, V., Boukos, N., Zergioti, I.., Fotakis, C., "Ultraviolet femtosecond, picosecond and nanosecond laser microstructuring of silicon: structural and optical properties," Appl. Opt. **47**(11), 1846–1850 (2008).
[11] Zhu, J., Yin, G., Zhao, M., Chen, D.., Zhao, L., "Evolution of silicon surface microstructures by picosecond and femtosecond laser irradiations," Appl. Surf. Sci. **245**(1-4), 102–108 (2005).
[12] Zorba, V., Alexandrou, I., Zergioti, I., Manousaki, A., Ducati, C., Neumeister, A., Fotakis, C.., Amaratunga, G. A. J., "Laser microstructuring of Si surfaces for low-threshold field-electron emission," Thin Solid Films **453-454**, 492–495 (2004).
[13] Her, T. H., Finlay, R. J., Wu, C.., Mazur, E., "Femtosecond laser-induced formation of spikes on silicon," Appl. Phys. A Mater. Sci. Process. **70**, 383–385 (2000).
[14] Tull, B. R., Carey III, J. E., Mazur, E., McDonald, J. P.., Yalisove, S. M., "Silicon surface morphologies after femtosecond laser irradiation," MRS Bull. **31**(08), 626–633, Cambridge Univ Press (2011).
[15] Crouch, C. H., Carey III, J. E., Warrender, J. M., Aziz, M. J., Mazur, E.., Génin, F. Y., "Comparison of structure and properties of femtosecond and nanosecond laser-structured silicon," Appl. Phys. Lett. **84**(11), 1850 (2004).
[16] Zuhlke, C. A., Anderson, T. P.., Alexander, D. R., "Formation of multiscale surface structures on nickel via above surface growth and below surface growth mechanisms using femtosecond laser pulses," Opt. Express **21**(7), 8460–8473 (2013).
[17] Zuhlke, C. A., Anderson, T. P.., Alexander, D. R., "Comparison of the structural and chemical composition of two unique micro/nanostructures produced by femtosecond laser interactions on nickel," Appl. Phys. Lett. **103**(12), 121603 (2013).
[18] Zuhlke, C. A., Anderson, T. P.., Alexander, D. R., "Fundamentals of layered nanoparticle covered pyramidal structures formed on nickel during femtosecond laser surface interactions," Appl. Surf. Sci. **21**(7), 8460–8473, Elsevier B.V. (2013).
[19] Kruse, C., Anderson, T., Wilson, C., Zuhlke, C., Alexander, D., Gogos, G.., Ndao, S., "Extraordinary shifts of the leidenfrost temperature from multiscale micro/nanostructured surfaces.," Langmuir (2013).
[20] Kruse, C. M., Anderson, T., Wilson, C., Zuhlke, C., Alexander, D., Gogos, G.., Ndao, S., "Enhanced pool-boiling heat transfer and critical heat flux on femtosecond laser processed stainless steel surfaces," Int. J. Heat Mass Transf. **82**, 109–116, Elsevier Ltd (2015).
[21] Zuhlke, C. A., Anderson, T. P.., Alexander, D. R., "Understanding the formation of self-organized micro/nanostructures on metal surfaces from femtosecond laser ablation using stop-motion SEM imaging," Proc. SPIE 8968, Laser-based Micro- Nanoprocessing VIII, U. Klotzbach, K. Washio, and C. B. Arnold, Eds., 89680C (2014).
[22] Zuhlke, C. A., "Control and understanding of the formation of micro/nanostructured metal surfaces using femtosecond laser pulses," ProQuest, University of Nebraska (2012).
[23] Vorobyev, A. Y.., Guo, C., "Femtosecond laser structuring of titanium implants," Appl. Surf. Sci. **253**(17), 7272–7280 (2007).
[24] Vorobyev, A. Y.., Guo, C., "Femtosecond laser surface structuring of biocompatible metals," Proc. SPIE **7203**, 72030O – 72030O – 8, Spie (2009).
[25] Fadeeva, E., Truong, V. K., Stiesch, M., Chichkov, B. N., Crawford, R. J., Wang, J.., Ivanova, E. P., "Bacterial retention on superhydrophobic titanium surfaces fabricated by femtosecond laser ablation," Langmuir, 3012–3019 (2011).
[26] Steele, A., Nayak, B. K., Davis, A., Gupta, M. C.., Loth, E., "Linear abrasion of a titanium superhydrophobic surface prepared by ultrafast laser microtexturing," J. Micromechanics Microengineering **23**(11), 115012 (2013).
[27] Moradi, S., Kamal, S., Englezos, P.., Hatzikiriakos, S. G., "Femtosecond laser irradiation of metallic surfaces: effects of laser parameters on superhydrophobicity.," Nanotechnology **24**(41), 415302 (2013).
[28] Bonse, J., Wrobel, J. M., Krüger, J.., Kautek, W., "Ultrashort-pulse laser ablation of indium phosphide in air," Appl. Phys. A Mater. Sci. Process. **72**(1), 89–94 (2001).
[29] Butt, H.-J., Roisman, I. V., Brinkmann, M., Papadopoulos, P., Vollmer, D.., Semprebon, C., "Characterization of super liquid-repellent surfaces," Curr. Opin. Colloid Interface Sci. **19**(4), 343–354, Elsevier Ltd (2014).
[30] Poetes, R., Holtzmann, K., Franze, K.., Steiner, U., "Metastable Underwater Superhydrophobicity," Phys. Rev. Lett. **105**(16), 166104 (2010).
[31] Kietzig, A.-M., Hatzikiriakos, S. G.., Englezos, P., "Patterned superhydrophobic metallic surfaces," Langmuir **25**(8), 4821–4827 (2009).

[32] Darmanin, T., De Givenchy, E. T., Amigoni, S.., Guittard, F., "Hydrocarbon versus fluorocarbon in the electrodeposition of superhydrophobic polymer films," Langmuir **26**(37), 17596–17602 (2010).
[33] Schulz, H., Leonhardt, M., Scheibe, H. J.., Schultrich, B., "Ultra hydrophobic wetting behaviour of amorphous carbon films," Surf. Coatings Technol. **200**, 1123–1126 (2005).
[34] Thieme, M., Streller, F., Simon, F., Frenzel, R.., White, a. J., "Superhydrophobic aluminium-based surfaces: Wetting and wear properties of different CVD-generated coating types," Appl. Surf. Sci. **283**, 1041–1050, Elsevier B.V. (2013).